



Encapsulation of bacterial cells in cytoprotective ZIF-90 crystals as living composites



H. Li^{a,f}, A. Kang^{a,f}, B. An^a, L.-Y. Chou^a, F.-K. Shieh^b, C.-K. Tsung^{c,**}, C. Zhong^{a,*,d,e}

^a Materials and Physical Biology Division, School of Physical Science and Technology, ShanghaiTech University, Shanghai 201210, China

^b Department of Chemistry, National Central University, Taoyuan 32001, Taiwan

^c Boston College Chemistry Department, Merkert Chemistry Center, 2609 Beacon St, Chestnut Hill, MA 02467, USA

ARTICLE INFO

Keywords:

Metal-organic framework
E. coli
 Living materials
 Encapsulation efficiency
 Cytoprotective cage

ABSTRACT

Exploiting metal-organic frameworks (MOFs) as selectively permeable shelters for encapsulating engineered cells to form hybrid living materials has attracted increasing attention in recent years. Optimizing the synthesis process to improve encapsulation efficiency (EE) is critical for further technological development and applications. Here, using ZIF-90 and genetically engineered *Escherichia coli* (*E. coli*) as a demo, we fabricated *E. coli*@ZIF-90 living composites in which *E. coli* cells were encapsulated in ZIF-90 crystals. We illustrated that ZIF-90 could serve as a protective porous cage for cells to shield against toxic bactericides including benzaldehyde, cinnamaldehyde, and kanamycin. Notably, the *E. coli* cells remained alive and could self-reproduce after removing the ZIF-90 crystal cages in ethylenediaminetetraacetic acid, suggesting a feasible route for protecting and prolonging the lifespan of bacterial cells. Moreover, an aqueous multiple-step deposition approach was developed to improve EE of the *E. coli*@ZIF-90 composites: the EE increased to $61.9 \pm 5.2\%$, in contrast with the efficiency of the traditional method ($21.3 \pm 4.4\%$) prepared with PBS buffer. In short, we develop a simple yet viable strategy to manufacture MOF-based living hybrid materials that promise new applications across diverse fields.

1. Introduction

Inspired by the natural preservation mechanisms of evolving protective armor to resist various external stresses, individual cells coated with artificial shells have been developed to enhance resistance against external environmental stress [1–4]. Biocompatible organic coatings such as polyelectrolytes [5–7], polydopamine [8,9], pyrogallols [10,11], and silk protein [12,13] have been widely applied for encapsulation of various cells to preserve cell viability and induce cell dormancy via layer-by-layer assembly. However, organic polymers are often not robust enough to provide rigorous and long-term protection for the cells [14]. To such ends, using biomimetic mineralization, inorganic materials such as calcium phosphate (CaP) [15], silica [16–18], titania [19], and cerium oxide (CeO₂) [20] have been incorporated into existing polymeric

coating layers on the cell surface with improved and prolonged mechanical strength. However, the removal or dissolution of those organic or inorganic shells is often carried out at harsh acid or base conditions, therefore causing permanent cell deaths [21]. Recently, owing to the brilliant physical/chemical stability, high biocompatibility, tunable permeation ability, and benign synthesis conditions [22–25], metal-organic frameworks (MOFs) become promising reliable shelters for storing and protecting bioactive matter (from simple biomolecules [26–31] to living cells [32–34]) under benign conditions. Notably, the zeolitic imidazolate framework 8 (ZIF-8) is among the most popular MOFs for cell encapsulation due to its biocompatibility and controllable degradation [29,35–39]. However, the polycrystalline ZIF-8 coating shells could not achieve complete coverage due to the cracks between polycrystalline MOF units. Such imperfect coverage thus could not

* Corresponding author.

** Corresponding author.

E-mail addresses: frank.tsung@bc.edu (C.-K. Tsung), chao.zhong@siat.ac.cn (C. Zhong).

^d Present Address: Center for Materials Synthetic Biology, Shenzhen Institute of Synthetic Biology, Shenzhen Institutes of Advanced Technology, Chinese Academy of Sciences, Shenzhen 518055, China

^e Present Address: CAS Key Laboratory of Quantitative Engineering Biology, Shenzhen Institute of Synthetic Biology, Shenzhen Institutes of Advanced Technology, Chinese Academy of Sciences, Shenzhen 518055, China

^f Contributed equally.

<https://doi.org/10.1016/j.mtbio.2021.100097>

Received 22 October 2020; Received in revised form 19 January 2021; Accepted 20 January 2021

Available online 4 February 2021

2590-0064/© 2021 The Author(s). Published by Elsevier Ltd. This is an open access article under the CC BY-NC-ND license (<http://creativecommons.org/licenses/by-nc-nd/4.0/>).

effectively provide protective roles for the cells against small toxic molecules such as (benzaldehyde), thereby eventually resulting in cell deaths when overexposed. Moreover, current approaches for direct observations of MOFs-cell living composites usually require pre-staining of living cells with chemical dyes, which are generally toxic to cells and might affect their pre-defined dynamic functions [33]. Thus better shelter systems and more biocompatible labeling tools are highly desirable for cell encapsulation.

Here, we developed a facile biocompatible approach for completely encapsulating living cell (*E. coli*) inside single-crystalline ZIF-90 particles under aqueous conditions via the one-pot approach. In addition, applying a genetically engineered *E. coli* strain that expressed mCherry (a red fluorescent protein), we demonstrated successful visualization of *E. coli*@ZIF-90 under microscopy without using specific chemical dyes to stain *E. coli* cells and ZIF-90. Notably, ZIF-90 could serve as a protective cage for *E. coli* cells to shield against toxic chemicals including benzaldehyde, cinnamaldehyde, and kanamycin. Besides, cytoprotective ZIF-90 cages can prolong cell lifespan by artificially inhibiting cell division, while retaining the protected cells' self-reproducing capacity after ZIF-90 removal. Significantly, compared to the conventional one-pot method, encapsulation efficiency (EE %, defined as the proportion of ZIF-90 crystals containing encapsulated cells to all the ZIF-90 particles, including those none cell-encapsulated empty ZIF-90 crystals in the system) was substantially improved to $61.9 \pm 5.2\%$ from $21.3 \pm 4.4\%$ through a multiple-step deposition (MSD) method. This multi-step deposition approach for high EE of MOF-based biocomposites can be applied for microencapsulation of other types of cells other than *E. coli* [40–42], providing a new approach to synthesize hybrid living materials with higher environment tolerance.

2. Materials and methods

2.1. Materials

Zinc nitrate hexahydrate ($\text{Zn}(\text{NO}_3)_2 \cdot 6\text{H}_2\text{O}$, 99%, Aladdin), Polyvinylpyrrolidone (PVP, Mw 24000, Aladdin), Imidazole-2-formaldehyde (ICA, 97%, Alfa Aesar), Phosphate buffered saline (PBS, powder, Abcone), Luria-Bertani (LB), Potassium chloride (KCl, Aladdin), Isopropyl-beta-D-thiogalactopyranoside (IPTG, Sigma), ethylenediaminetetraacetic acid (EDTA, Aladdin), Kanamycin (Aladdin), sodium chloride (NaCl, Aladdin), menzaldehyde (Aladdin), cinnamaldehyde (Aladdin), tris(hydroxymethyl)aminomethane (Adamas), TBS buffer (8 g NaCl, 0.2 g KCl and 3 g Tris-base dissolved in 1 L DI water, adjusting pH = 7.4 with HCl), DMF (Aladdin), CH_2Cl_2 (Aladdin) CDCl_3 (Aladdin). All aqueous solution and DI water were sterilized before further use. All reagents and solvents used were of commercially available reagent grade and were used without any additional purification.

2.2. Characterization

Scanning electron microscope (SEM) images were acquired on a JEOL JSM - 6010 Plus/LA and a JEOL JSM-7800F Prime to examine the crystal size and morphology. Samples were coated with Au for 30 s using an SBC-12 sputter coater. Samples for transmission electron microscopy (TEM) were dispersed in methanol. A droplet of the suspension was transferred onto a carbon-coated copper grid. Transmission electron microscope (TEM) images were acquired on JEOL JEM-2100 Plus and JEOL JEM-1400 Plus operated at 200 kV and 120 kV, respectively. SEM samples were prepared by dropping suspensions onto the silicon wafer and air-dried for 12 h. SEM was performed on a JSM 7800F Prime field-emission SEM. Fluorescence microscopy was performed on ZEISS Axio Imager Z2. Thermogravimetric analyses (TGAs) were performed on PerkinElmer TGA 8000 with a heating rate of $20\text{ }^\circ\text{C}/\text{min}$ from ambient to $650\text{ }^\circ\text{C}$. Powder X-ray diffraction patterns (PXRD) were acquired on a Bruker D8 Advance diffractometer with $\text{Cu K}\alpha$ (1.54 \AA) radiation. The scan speed was 0.2 s per step. The OD_{600} of bacteria was obtained by

BioTek Cytation 5. Attenuated total reflection (ATR)-Fourier transform infrared (FTIR) spectra were measured using a PerkinElmer Spectrometer Frontier in the range of $400\text{--}4,000\text{ cm}^{-1}$ at a resolution of 1 cm^{-1} . Nuclear magnetic resonance (NMR): $^1\text{H-NMR}$ spectra were recorded using a Bruker AV NEO 400 M spectrometer or Bruker AVIII HD 500 M spectrometer under room temperature.

2.3. Engineered *E. coli* for IPTG-induced expression of red fluorescent proteins

E. coli (BL21 DE3) was genetically modified by introducing a mCherry-expression plasmid under the regulation of the T7 promoter in pET22b plasmid. Upon IPTG induction, the engineered bacteria produced fluorescent proteins emitting red fluorescence (610 nm) under 580 nm light excitation.

2.4. Bacterial culture

Seed cultures were inoculated from frozen glycerol stocks into 5 mL LB-Miller medium containing carbenicillin antibiotics at $50\text{ }\mu\text{g}/\text{mL}$ concentrations. Seeds were grown for 24 h at $37\text{ }^\circ\text{C}$ with shaking at 220 rpm.

2.5. One-pot aqueous synthesis of pure ZIF-90

In a 50 mL glass vial, 720 mg imidazole-2-formaldehyde and 75 mg PVP were dissolved in 25 mL deionized water, stirred and heated in a metal bath of $80\text{ }^\circ\text{C}$ to dissolve completely, and then cooled to $40\text{ }^\circ\text{C}$. Zinc nitrate solution (0.62 M) of 2.5 mL was added and stirred for 5 min (500 rpm) on a magnetic stirrer. The product was washed twice with water and collected by centrifugation.

2.6. Synthesis of *E. coli*@ZIF-90 by one-pot (with PBS)

Imidazole-2-formaldehyde of 360 mg and 37.5 mg of PVP were dissolved in 12.5 mL deionized water, stirred, and heated in a metal bath of $80\text{ }^\circ\text{C}$ to dissolve completely and then cooled to $40\text{ }^\circ\text{C}$. Then, 1 mL *E. coli* ($\text{OD}_{600} = 0.8$, suspended in PBS solution) firstly induced by IPTG for 3 h, then added to the reaction system and mixed homogeneously. Next, 1.25 mL 0.62 M zinc nitrate solution was added and stirred for 5 min (500 rpm) on a magnetic stirrer. The product was washed twice with water and collected by centrifugation.

2.7. Synthesis of *E. coli*@ZIF-90 embedded in polymer to form *E. coli*@ZIF-90@polymer

To facilitate sectioning of *E. coli*@ZIF-90 for direct observation of *E. coli* trapped in ZIF-90, we used polyimide (PI) to fix the sample. The preparation of *E. coli*@ZIF-90@polymer followed a protocol published in previous work by Wang et al. [43] The process started with PI grafting onto *E. coli*@ZIF-90 by a stepwise growth polymerization process of equimolar 4,4'-phthalic anhydride (ODPA)-2,4,6-trimethyl-p-phenylenediamine (DAM), followed by an in situ chemical imidization process. After that, *E. coli*@ZIF-90 was embedded into PIs to form *E. coli*@ZIF-90@polymer. For preparing *E. coli*@ZIF-90@polymer membranes, 3 wt% polymer (ODPA-DAM) in dry CH_2Cl_2 solution was filtered through a 0.45 mm PTFE filter onto a casting tray and 2 mg *E. coli*@ZIF-90 powder was added. The tray consisted of a glass ring attached to a level glass plate with the epoxy sealant. After slow evaporation of the solvent, the membranes were peeled off from the glass plate and dried overnight to remove residual solvent. The samples were then immersed in liquid nitrogen for 10 min, and then the stiffness samples were broken off with forceps.

2.8. Thermogravimetric analyses

TGAs were performed on PerkinElmer TGA 8000. First, the TGA

profile of the sample was obtained by heating it from ambient temperature to 100 °C at the rate of 20 °C/min and the temperature kept at 100 °C for 10 min at N₂ atmosphere to remove the solvent. Then the temperature raised to 650 °C at the rate of 20 °C/min at O₂ atmosphere.

2.9. ATR-FTIR measurement of *E. coli*@ZIF-90 composites

The FTIR spectra were collected on a PerkinElmer Spectrometer Frontier equipped with an ATR single-reflection diamond ATR module. Then, 20 mL *E. coli* (OD₆₀₀ = 0.8) was washed by using 3 times volume of deionized water and then dried up. After that, 10 mg *E. coli*@ZIF-90 composites and 10 mg pure ZIF-90 crystals were dried up in 65 °C ovens for 8 h before use for further characterization.

2.10. Protective effects of the *E. coli*@ZIF-90 composites under different chemical agents

1 mL of *E. coli*@ZIF-90 (one-pot, PBS) sample and 0.5 mL of free *E. coli* cells (OD₆₀₀ = 0.8) were put into a 1.5 mL centrifuge tube and centrifuged (8,000 rpm, 3 min) to remove the supernatant. A mixed organic solution consisting of 0.5 mL cinnamaldehyde and 0.5 mL DI water was added to the precipitate. Then the precipitate and solvent were mixed homogeneously with a pipette. The mixture was gently shaken at room temperature (25 °C) for 6 h. In a similar procedure, a mixed organic solution consisting of 0.5 mL benzaldehyde and 0.5 mL DI water was also used in this system to test the effectiveness of protective ZIF-90 crystals.

2.11. ¹H-NMR spectrum of cinnamaldehyde and benzaldehyde

To rule out the possibility that aldehydes may react with ZIF-90 and thus lose their cytotoxicity, we performed ¹H-NMR tests on the supernatants of cinnamaldehyde-ZIF-90 and benzaldehyde-ZIF-90 mixtures (following the same condition of *E. coli*@ZIF-90 treated by cinnamaldehyde and benzaldehyde). The isometric mixture of cinnamaldehyde and deionized water was added to 10 mg ZIF-90 and then the sample was kept in a shaker for 6 h. After that, 50 μL supernatant of cinnamaldehyde-ZIF-90 was added to 0.5 mL CDCl₃ and then the sample was tested on ¹H-NMR. The ¹H-NMR spectrum for the benzaldehyde-ZIF-90 sample was carried out using a similar procedure.

2.12. Self-regenerating capacity assessment of *E. coli* cells after ZIF-90 crystals removal

The *E. coli*@ZIF-90 (one-pot) composites were prepared as described previously. The composites were treated with kanamycin (1:100, shaking at 37 °C) for at least 5 h to kill the free *E. coli* outside of ZIF-90. After treatment with 10 μL kanamycin, the sample was washed by deionized water for three times, and then the supernatant of the sample was cultivated in LB to test whether kanamycin could kill all free *E. coli* cells. Then, 10 mL 100 mM EDTA was used to remove the ZIF-90 crystals from *E. coli*@ZIF-90 through dissolution. After the *E. coli*@ZIF-90 was treated by EDTA, the sample was washed by using deionized water three times, and then the released *E. coli* cells were resuspended in 2 mL deionized water. About 5 μL of the resuspension containing *E. coli* cells as seeds were cultivated in LB solution at 37 °C (220 rpm) to assess the self-regenerating capacity of the deprotected cells.

2.13. Synthesis of ZIF-90 crystals in the presence of different buffers

The influence of different buffers on the size of ZIF-90 under one-pot synthesis conditions was probed. Briefly, 1 mL of different types of buffers (TBS, Tris-HCl) added to the precursors (mixtures of ICA and PVP) was homogeneously stirred for 5 min before the zinc nitrate solution was added. The samples were washed by using deionized water 3 times, and then dried up in 80 °C ovens overnight for further characterization.

2.14. Synthesis of *E. coli*@ZIF-90 by one-pot approach (without PBS).

Imidazole-2-formaldehyde of 360 mg and 37.5 mg of PVP were dissolved in 12.5 mL deionized water, stirred, and heated in a metal bath of 80 °C to dissolve completely and then cooled to 40 °C. After that, 1 mL *E. coli* (OD₆₀₀ = 0.8, suspended in DI water) was added to the reaction system and mixed well. Next, 1.25 mL 0.62 M zinc nitrate solution was added and stirred for 5 min (500 rpm) on a magnetic stirrer. The product was washed twice with water and collected by centrifugation.

2.15. Synthesis of *E. coli*@ZIF-90 through MSD

First, bacteria were immersed in 3 mL low concentration ICA solution (86.5 mg ICA, 18 mg PVP, and 6 mL DI H₂O) for 10 min, and then 1 mL low concentration zinc ion solution (139.2 mg Zn(NO₃)₂·6H₂O and 1.5 mL H₂O) was added. Second, 3 mL low concentration ICA solution and 0.5 mL low concentration zinc ion solution were sequentially added every 2 min. After the reaction was completed, the mixture was centrifuged, and the supernatant was removed. Third, a 4 mL high concentration ICA solution (360.3 mg ICA, 75 mg PVP, 12.5 mL H₂O and 1 mL PBS solution) was added to the precipitate for 5 min. Then 0.5 mL zinc ion solution (278.3 mg Zn(NO₃)₂·6H₂O and 1.5 mL DI H₂O) was added. 4 mL high concentration ICA solution and 0.5 mL high concentration zinc ion solution were sequentially added every 0.5 min. This operation was repeated twice. Finally, the sample was centrifuged and washed twice with DI water.

2.16. Etching *E. coli*@ZIF-90 for morphological characterization

Etching of *E. coli*@ZIF-90 composites prepared through MSD was carried out by resuspension of the samples in 5 mL LB with shaking at 220 rpm at 37 °C for 4 h. The samples were then collected for characterization by TEM to exam the formed structures.

3. Results and discussion

3.1. Living cells encapsulated in single-crystalline ZIF-90 crystal

To facilitate observation of *E. coli*@ZIF-90 (referring to *E. coli* encapsulated in ZIF-90 particles) living composites under the fluorescence microscope, a genetically engineered *E. coli* strain that expresses red fluorescent protein (RFP, mCherry) induced by IPTG was applied in this study (Fig. S1). As the molecular size of IPTG (C₉H₁₈O₅S, ~8 Å) is significantly larger than that of the ZIF-90 pore (~3.7 Å), IPTG could not penetrate through the MOFs to reach the encapsulated *E. coli*. To such an end, IPTG was added to induce *E. coli* for fluorescent protein expression before encapsulation. For preparing *E. coli*@ZIF-90 living composites, zinc nitrate hexahydrate solution (Zn(NO₃)₂·6H₂O, 0.62 M) was added into the appropriate amount of mixture containing imidazole-2-carbaldehyde (ICA, 0.3 M), polyvinylpyrrolidone (PVP, 10 wt%) and the genetically engineered *E. coli* cells (OD₆₀₀ = 0.8, homogeneously pre-distributed in 1 mL PBS buffer solution). Upon thorough stirring followed by washing with DI water, *E. coli*@ZIF-90 composites could be obtained (Fig. 1a) using this one-pot method. As the engineered bacteria could emit strong red fluorescence (610 nm) after excitation by 580 nm green light (Fig. 1b), the cells that were encapsulated into ZIF-90 could be easily detected using the fluorescence microscope (Fig. 1c, Video S1). Based on fluorescence images, about 21.3 ± 4.4% of the formed ZIF-90 crystals had been found to contain mCherry-producing *E. coli* (Fig. S2, Table S1). Morphological characterization of *E. coli*@ZIF-90 using scanning electron microscopy (SEM) further confirmed that engineered *E. coli* cells could be encapsulated into ZIF-90 with intact MOF structural integrity (Fig. 1d). To investigate the interfacial boundary between *E. coli* and ZIF-90 and verify whether *E. coli* is completely encapsulated in ZIF-90, we performed SEM observations of the cross-section of the *E. coli*@ZIF-90 through embedding the sample in polyimide. As shown in

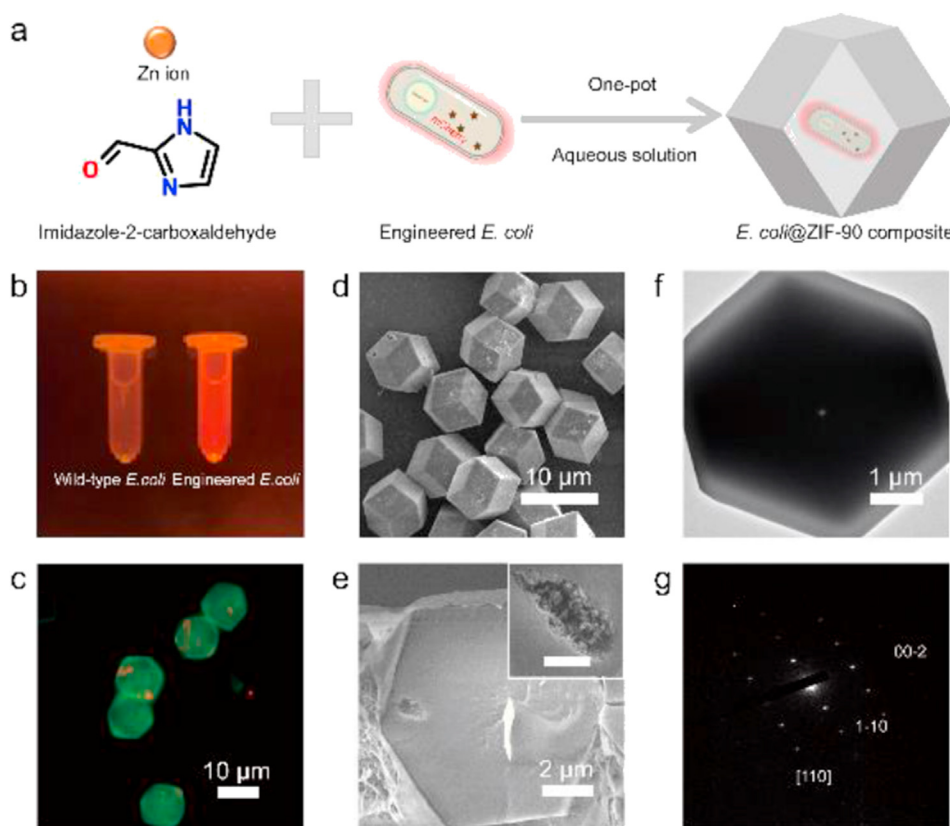


Fig. 1. (a) Synthetic scheme of the engineered *Escherichia coli* (*E. coli*) encapsulated in ZIF-90 to produce *E. coli*@ZIF-90 living composites. (b) Comparison of the wild-type *E. coli* (left) and engineered *E. coli* (right) that can express red fluorescent protein under excitation at 580 nm; (c) Fluorescent microscope image of the *E. coli*@ZIF-90; (d) SEM image of the *E. coli*@ZIF-90 (one-pot); (e) SEM image of the interfacial cross-section between engineered *E. coli* and ZIF-90 (via the one-pot approach), the scale bar of zoom in cross-section image is 500 nm; (f) TEM image of the *E. coli*@ZIF-90 (via the one-pot approach); (g) TEM diffraction of the *E. coli*@ZIF-90 (via the one-pot approach).

Fig. 1e, the SEM image revealed that the *E. coli* cell was tightly trapped inside the ZIF-90 crystal. Besides, TEM imaging of *E. coli*@ZIF-90 clearly showed the well-defined rhombic dodecahedron of ZIF-90 crystals (Fig. 1f) and the corresponding TEM diffraction pattern further demonstrated its single-crystalline feature (Fig. 1g), whose crystal plane [110] agrees with that of pure single-crystalline ZIF-90. TGA were performed on PerkinElmer TGA 8000 as indirect evidence to support that engineered *E. coli* cells were successfully encapsulated in ZIF-90 particles. The samples collected for TGA characterization were pre-treated with harsh solutions to ensure that cells adhering to the outer surface were washed away, and then TGA was carried out by heating it from ambient temperature to 650 °C. Intriguingly, the TG profile of the sample showed the living composites sample, compared with pure ZIF-90 crystal sample, had a significant weight descend at around 300 °C, with mass percentage decreased from about 70% to 50%, indirectly showing that the pronounced weight loss is correlated with the encapsulated cells in ZIF-90 (Fig. S3).

3.2. Interaction between *E. coli* cells and ZIF-90 crystals

Although several reports indicated close interactions between various living cells and MOFs [34,44,45], much more needs to be investigated at the interface between organisms and different types of MOFs nano-materials. To exam whether *E. coli* cells simply adhere to the surface of ZIF-90 or have possible interaction with ZIF-90, we used ATR-FT-IR spectroscopy to characterize the interaction between *E. coli* and ZIF-90 crystals. As shown in Fig. 2a, the peak of original *E. coli* at 1,628 cm^{-1} corresponds to the stretching vibrations of C–N and C=O in the protein amide, and the absorption peaks at 1,520 cm^{-1} and 1,451 cm^{-1} represent the C–N vibrations of amide II in the protein-peptide bond [46]. The vibrational band at 1,219 cm^{-1} represents the asymmetric stretching vibration of the diphosphate group P=O. The aforementioned data are consistent with the previous reports about extracellular polymeric substances of bacteria [46,47]. The spectrum of as-synthesized

ZIF-90 shows peaks identical to those in previous reports [48,49], providing further evidence for the correct chemical structure. The most representative band at 1,668 cm^{-1} as indicated by the arrow corresponds to the aldehyde stretch of the imidazole ligands. In contrast, in the *E. coli*@ZIF-90 sample, $\nu_{\text{P=O}}$ stretching frequency at 1,219 cm^{-1} was no longer detected, which might be ascribed to the formation of Zn–O–P between the inorganic crystal and the bacterial surface. In addition, compared with the spectrum of *E. coli*@ZIF-90 in Fig. 2b, the C=O band of the pure MOF crystal sample is red-shifted from 1,668 cm^{-1} to 1,

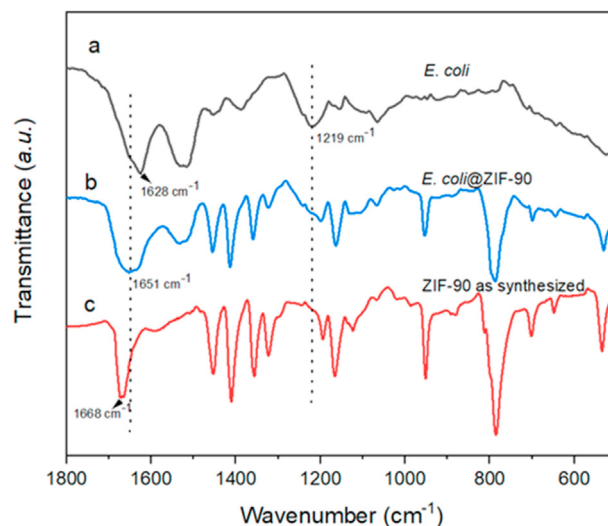


Fig. 2. ATR-FTIR spectrum of (a) intact *E. coli* cells (20-mL OD₆₀₀ = 0.8 *E. coli* washed by deionized water 3 times, then dried up); (b) *E. coli*@ZIF-90 composites after drying; (c) pure ZIF-90 crystals after drying. All samples were dried in 65 °C ovens for 8 h. ATR, attenuated total reflection.

651 cm^{-1} , implying that the Zn clusters on the *E. coli* surface in the bacteria-MOF composites have metal-coordination interactions with C=O and P=O from phosphate groups of teichoic acid and glycoproteins on the cell surface [33,34,50]. Collectively, the FT-IR results indicate that specific interactions indeed occur between the living bacteria and ZIF-90 crystals, rather than just simply adhering to the interior wall of the MOF.

3.3. Self-regeneration assessment of *E. coli* cells after cytoprotective ZIF-90 removal

Previous studies showed that MOF materials could provide excellent protection for biomolecules against various deteriorating conditions and the protected biomolecules showed up to 10-fold enhanced stability compared to unprotected biomolecules [51–53]. To verify whether ZIF-90 can protect cells under various harsh conditions, two common bactericides, benzaldehyde and cinnamaldehyde, were applied as toxic chemicals to challenge the environmental tolerance of *E. coli*@ZIF-90 composites in this study (Fig. 3a). To verify the real protective effect of the MOF materials, extra free *E. coli* were simultaneously added and mingled with *E. coli*@ZIF-90 composite samples. Engineered *E. coli* cells that express mCherry treated under non-toxic conditions were used as a control group (Fig. 3b). After treatment with benzaldehyde (Fig. 3c) and cinnamaldehyde (Fig. 3d), the free cells completely lost fluorescence. In contrast, the cells encapsulated in the ZIF-90 porous shell could retain the fluorescent signals. These data suggest ZIF-90 cages can help to protect the *E. coli* cells against unfriendly environments. Besides, to rule out the possibility that aldehydes may react with ZIF-90 and thus lessen or even lose their cytotoxicity to the cells, we also performed $^1\text{H-NMR}$ tests on the supernatants of cinnamaldehyde-ZIF-90 and benzaldehyde-ZIF-90 mixtures (under the same condition of *E. coli*@ZIF-90 treated by cinnamaldehyde and benzaldehyde). The supernatant of benzaldehyde-ZIF-90 compounds show no extra peaks on the $^1\text{H-NMR}$ spectrum after 6 h of shaking treatment (Figs. S4a and b). Note that similar results also could

be obtained for the cinnamaldehyde-ZIF-90 sample (Figs. S5a and b). These data suggest that ZIF-90 does not react with cinnamaldehyde and benzaldehyde, thus eliminating the possibility that their toxic effects can be removed by reacting with ZIF-90 crystals. Conceivably, the pore size of ZIF-90 ($\sim 3.7 \text{ \AA}$) is much smaller than the molecular sizes of cinnamaldehyde ($\sim 8 \text{ \AA}$) and benzaldehyde ($\sim 6 \text{ \AA}$), therefore preventing the penetration of these toxic reagents into the internal parts of the crystals and eventually protecting *E. coli* cells from the cytotoxicity of cinnamaldehyde and benzaldehyde with their physical barriers.

In addition to broad-spectrum bactericides (benzaldehyde and cinnamaldehyde), kanamycin, a common antibiotic, was also applied to test the protective effect of ZIF-90. Note that kanamycin can completely disrupt the *E. coli* cell wall causing its almost 100% mortality (Fig. 3e). In contrast, both the zinc nitrate solution and the mixture of ICA and PVP slightly reduced the amounts of *E. coli* after exceeding 16 h incubation (Fig. 3e), indicating that the precursors of ZIF-90 would affect the proliferation of *E. coli* cells to some extent but not fatal enough to the viability of *E. coli* cells. To verify whether the encapsulated *E. coli* cells are still alive after treatment with kanamycin, the *E. coli*@ZIF-90 composites were incubated in a medium containing kanamycin for 5 h. As shown in Fig. 3g, after treatment of *E. coli*@ZIF-90 with kanamycin, the OD_{600} value of the supernatant does not change compared with the control group (blank LB broth), implying that the non-encapsulated free *E. coli* cells were entirely killed by kanamycin. Then ethylene diamine tetraacetic acid (EDTA) was used to dissolve the structure of ZIF-90 to release *E. coli* cells. Note that either EDTA or ZIF-90 crystal has a negligible impact on *E. coli* cells' viability (Fig. 3f). After MOF cage dissolution, the *E. coli* cells could restore self-reproducing capacity (Fig. 3g). Thus, these results demonstrated that *E. coli* cells were encapsulated completely in ZIF-90 and ZIF-90 crystal could serve as a protective cage to help shield the engineered *E. coli* against the damages caused by various toxic reagents through physical isolation. Artificial cytoprotective shell engenders extended cell lifetimes and therefore underpins the advancement of

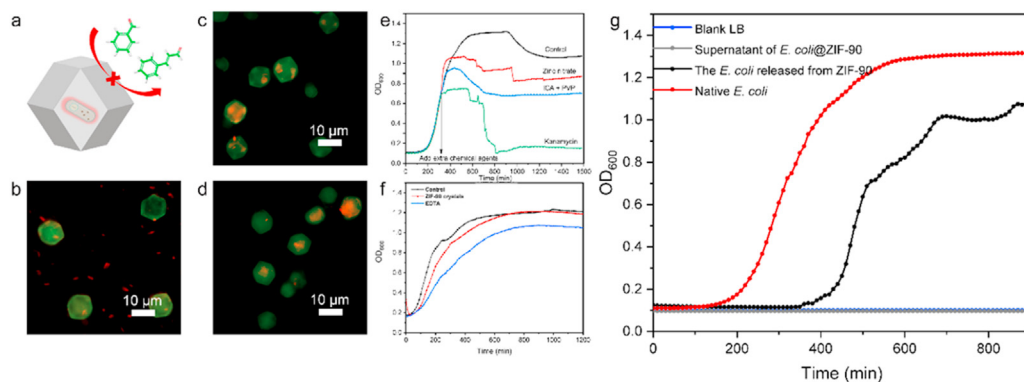


Fig. 3. (a) Schematic of ZIF-90 protecting bacteria from bactericides; (b) Mixture of *E. coli*@ZIF-90 and free *E. coli* cells without chemical treatments; (c) Mixture of *E. coli*@ZIF-90 and free *E. coli* cells after treatment with benzaldehyde; (d) Mixture of *E. coli*@ZIF-90 and free *E. coli* cells after treatment with cinnamaldehyde; (e) 5 μL *E. coli* as seeds were cultivated in 200 μL LB solution for 5 h, then 20 μL of the precursor of ZIF-90 crystals and kanamycin were added. The control group was only added with 20 μL deionized water after culture for 5 h. Experiments were performed in triplicates; (f) 10 μL ZIF-90 crystals (2 mg/mL) and EDTA (100 mM) were simultaneously added with 5 μL *E. coli* cells into 200 μL LB solution and then cultivated at 37 $^{\circ}\text{C}$ for 20 h. Experiments were performed in triplicates; (g) *E. coli* growth measurement (OD_{600}) for native (red circles) and the *E. coli* after the removal of MOFs cage by EDTA (black circles). Blank LB broth as a control group and the growth curve of *E. coli*@ZIF-90 supernatant was treated with kanamycin for 5 h to remove the free *E. coli* cells outside of ZIF-90. Experiments were performed in triplicate.

engineering strategies toward governing cell division, proliferation, and differentiation [7,54–56]. The use of MOF cages to enhance the survival capability of living cells under harmful environment and to prolong cell lifespan by artificially inhibiting cell division without significantly affecting the activity of the cells in the growth state may expand the application scenarios of engineered living cells.

3.4. Effect of PBS buffer on EE of *E. coli*@ZIF-90

To understand how bacterial cells were encapsulated in ZIF-90, the influences of PBS buffer and PVP on cell encapsulation were probed. We first compared the encapsulation in the presence and absence of PBS during the hybrid material fabrication process. As shown in Fig. 4b, the EE of *E. coli*@ZIF-90 in the absence of PBS decreased to $5.1 \pm 0.75\%$ (Fig. S6, Table S2) from $21.3 \pm 4.4\%$. The influence of PBS buffer on EE might be due to a slower ZIF-90 growth rate. The phosphate ions in PBS buffer likely serve as a modulator to slow down ZIF-90 crystals' growth. The decreased nucleation and growth rate of ZIF-90 in the PBS buffer could allow thorough time for forming initial nucleation MOF sites on the surface of *E. coli* cells, eventually resulting in more *E. coli* cells encapsulated in ZIF-90 particles. To verify the hypothesis of the buffer can influence the growth process of ZIF-90, different types of buffers (TBS and Tris-HCl) were investigated. As shown in Figs. S7a–c, the size of ZIF-90 increased with TBS buffer, demonstrating that TBS buffer slowed down the growth rate of ZIF-90 and resulted in a larger ZIF-90 particle. However, when Tris-HCl was used, no significant change for the size of ZIF-90 was observed (Fig. S7d). Therefore, it is believed that Tris-HCl has no noticeable effect on the growth process of ZIF-90, yet TBS plays a similar role as PBS in modulating the growth rate of ZIF-90 crystals.

We next assessed the role of PVP on cell encapsulation. Under the one-pot condition for synthesis of ZIF-90 crystals, well-defined ZIF-90 crystals could not be obtained without PVP (Fig. S8), indicating that the PVP is indeed needed for the formation of ZIF-90 crystals. Therefore, PVP is not

only important for the encapsulation but also necessary for ZIF-90 growth.

3.5. EE of *E. coli*@ZIF-90 improved by MSD

Based on the understanding that decreasing the growth rate of ZIF-90 is beneficial to improve the EE of *E. coli*@ZIF-90, a MSD approach toward decreasing the nucleation and growth rate of ZIF-90 particles was thus designed and applied for improving the EE % of *E. coli*@ZIF-90 (Fig. 4a). The process of preparing a single ZIF-90 crystal was accordingly divided into a five-step deposition. Specifically, *E. coli* cells resuspended in ICA (0.15 M) were mixed with appropriate PVP for a short time, followed by the addition of Zn (NO)₃·6H₂O to prepare the first-layer MOF-coated living hybrid materials. The resultant composites then served as seeds to produce multi-layer MOF-coated composites using a similar protocol with another four continuous steps. As the nucleation and growth rate of ZIF-90 particles could be practically decreased by a lower concentration of the precursors in each step, resulting in a higher possibility to trap *E. coli* cells in the MOF particles. As shown in Fig. 4d, most ZIF-90 particles successfully encapsulated *E. coli* cells. Compared with the one-pot method (Figs. 1c and 4b), almost no *E. coli* cells were absorbed on the surface of ZIF-90, implying the free *E. coli* cells could be removed by DI water during the several washing steps. The Video S2 formed by confocal fluorescence microscope of *E. coli*@ZIF-90 by MSD also confirmed that engineered *E. coli* cells were fully encapsulated in the single ZIF-90 particles. Mathematical statistical analysis shows that the *E. coli*@ZIF-90 composites prepared by the MSD approach had an EE of $61.9 \pm 5.2\%$ (Fig. S9, Table S3), substantially higher than the one-pot method, either in the absence of PBS Buffer ($5.1 \pm 0.75\%$) or in the presence of PBS buffer ($21.3 \pm 4.4\%$) (Fig. 4h). Interestingly, despite multiple steps involved, those steps did not affect the general rhombic dodecahedron morphology of the *E. coli*@ZIF-90 (Fig. 4e). However, these particles exhibited multilayered structures arising from the multiple

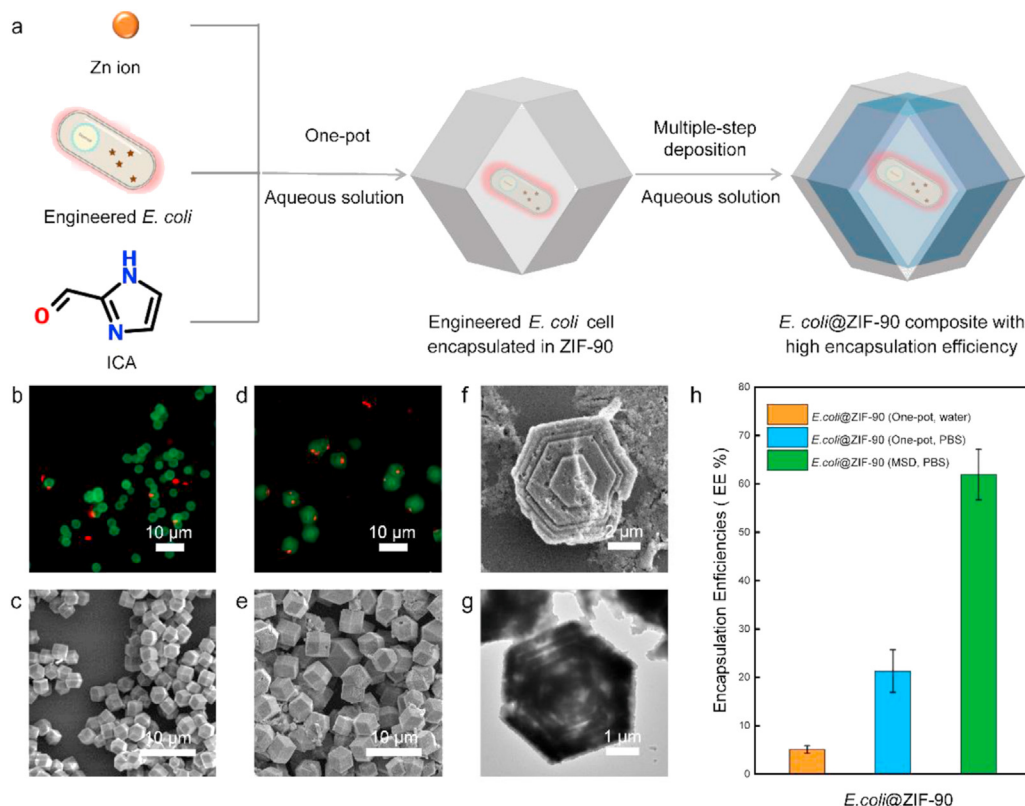


Fig. 4. (a) Synthetic scheme showing a multiple-step deposition (MSD) approach was applied to improve encapsulation efficiencies (EE %) of *E. coli*@ZIF-90; (b) Fluorescent microscope images of *E. coli*@ZIF-90 (one-pot, without PBS); (c) SEM image of *E. coli*@ZIF-90 (one-pot, without PBS); (d) Fluorescent microscope image of *E. coli*@ZIF-90 (MSD); (e) SEM image of *E. coli*@ZIF-90 (MSD); (f) SEM image of the cross-section of *E. coli*@ZIF-90 (MSD); (g) TEM image of *E. coli*@ZIF-90 (MSD) with LB etching for 4 h; (h) Encapsulation efficiency (EE %) of *E. coli*@ZIF-90 by different preparation approaches.

crystallization steps, as revealed by both SEM image (Fig. 4f) and TEM image (Fig. 4g). Despite those morphological differences, the crystal structures of ZIF-90 and *E. coli*@ZIF-90 (one-pot, MSD) determined by PXRD were identical (Fig. S10), and both were consistent with that of the simulated ZIF-90 structures (data from CCDC). Collectively, these results revealed that the EE of *E. coli*@ZIF-90 could be improved by this MSD approach, and the structure of multilayer ZIF-90 is consistent with pure ZIF-90 particles (one-pot). The multistep deposition for MOF-based biocomposites with improved EE% thus would provide a more practical approach for protecting cells against harsh conditions.

4. Conclusions

In summary, a facile and aqueous solution-based one-pot approach has been developed to produce living cells encapsulated in the ZIF-90 particles. Compared with free *E. coli* cells, the fabricated *E. coli*@ZIF-90 composites exhibited enhanced tolerance against toxic bactericides including benzaldehyde, cinnamaldehyde, and kanamycin. Notably, after the removal of ZIF-90, the *E. coli* cells remained alive and retained self-regenerating capacity. Subsequently, an aqueous MSD approach was developed to improve the EE of the *E. coli*@ZIF-90 composites.

The fabrication of living cell-MOF composite with enhanced EE provides new insights into the future development of hybrid living functional materials. By adjusting the MOF components and synthesis steps, it is possible to endow MOF materials with a variety of structures and functions (e.g., catalysis, electrical conductivity, adsorption, etc.) [57, 58]. Through synthetic biology, living systems (bacteria, fungi, mammalian cells, and so on) can also be engineered with a variety of user-defined capabilities [59]. The integration of MOF and living systems can effectively combine the advantages of both, and the resulting materials may show enhanced application potentials [24]. For example, the integration of a MOF that adsorbs uranium ions with a bacterium that specifically mineralizes uranium is expected to efficiently collect rare metals from the environment. Furthermore, by encasing a living strain expressing hydrogen-producing enzymes or high value-added metabolites in a MOF that can absorb solar energy to provide reducing forces, the functional properties of both can be better exploited to produce clean energy or fermentation products from solar energy. In addition, in stem cell biology, safety concerns are on the top priority focusing on contamination of a cell population by immature stem cells that can proliferate in an uncontrolled manner, forming tumors [60]. Encapsulating cells with MOFs offers an ideal tool for isolating individual cells from the population while retaining their potential differentiation and functionality.

Data availability

All experimental data within the article and its Supporting Information are available from the corresponding author upon reasonable request.

Declaration of competing interest

The authors declare that they have no known competing financial interests or personal relationships that could have appeared to influence the work reported in this paper.

Acknowledgments

This work was supported by the National Key R&D Program of China (grant nos. 2020YFA0908100) and National Natural Science Foundation of China (No. U1932204). F.-K. S. would like to thank the Ministry of Science and Technology, Taiwan for the funding support (MOST 107-2223-M-008 -008 -MY2). L.-Y. C. would like to thank the Shanghai natural science funding support (Grant No. 18ZR1425300).

Appendix A. Supplementary data

Supplementary data to this article can be found online at <https://doi.org/10.1016/j.mtbio.2021.100097>.

References

- [1] S.H. Yang, D. Hong, J. Lee, E.H. Ko, I.S. Choi, *Small* 9 (2013) 178–186.
- [2] J. Lee, H. Cho, J. Choi, D. Kim, D. Hong, J.H. Park, S.H. Yang, I.S. Choi, *Nanoscale* 7 (2015) 18918–18922.
- [3] S.H. Yang, S.M. Kang, K.B. Lee, T.D. Chung, H. Lee, I.S. Choi, *J. Am. Chem. Soc.* 133 (2011) 2795–2797.
- [4] I. Drachuk, O. Shchepelina, M. Lisunova, S. Harbaugh, N. Kelley-Loughnane, M. Stone, V.V. Tsukruk, *ACS Nano* 6 (2012) 4266–4278.
- [5] A.L. Hillberg, M. Tabrizian, *Biomacromolecules* 7 (2006) 2742–2750.
- [6] N.G. Veerabadrán, P.L. Goli, S.S. Stewart-Clark, Y.M. Lvov, D.K. Mills, *Macromol. Biosci.* 7 (2007) 877–882.
- [7] W.Y. Li, T. Guan, X.S. Zhang, Z.Y. Wang, M. Wang, W. Zhong, H. Feng, M. Xing, J.M. Kong, *ACS Appl. Mater. Interfaces* 7 (2015) 3018–3029.
- [8] B. Wang, G.C. Wang, B.J. Zhao, J.J. Chen, X.Y. Zhang, R.K. Tang, *Chem. Sci.* 5 (2014) 3463–3468.
- [9] B.J. Kim, T. Park, H.C. Moon, S.Y. Park, D. Hong, E.H. Ko, J.Y. Kim, J.W. Hong, S.W. Han, Y.G. Kim, I.S. Choi, *Angew. Chem. Int. Ed.* 53 (2014) 14443–14446.
- [10] J.Y. Kim, H. Lee, T. Park, J. Park, M.H. Kim, H. Cho, W. Youn, S.M. Kang, I.S. Choi, *Chem. Asian J.* 11 (2016) 3183–3187.
- [11] H.M. Pan, S.Y. Chen, T.S. Jang, W.T. Han, H.D. Jung, Y.N. Li, J.H. Song, *Biofabrication* (2019) 11.
- [12] I. Drachuk, M.K. Gupta, V.V. Tsukruk, *Adv. Funct. Mater.* 23 (2013) 4437–4453.
- [13] I. Drachuk, O. Shchepelina, S. Harbaugh, N. Kelley-Loughnane, M. Stone, V.V. Tsukruk, *Small* 9 (2013) 3128–3137.
- [14] G.C. Wang, L.J. Wang, P. Liu, Y. Yan, X.R. Xu, R.K. Tang, *Chembiochem* 11 (2010) 2368–2373.
- [15] B. Wang, P. Liu, W. Jiang, H. Pan, X. Xu, R. Tang, *Angew. Chem. Int. Ed. Engl.* 47 (2008) 3560–3564.
- [16] J. Lee, J. Choi, J.H. Park, M.H. Kim, D. Hong, H. Cho, S.H. Yang, I.S. Choi, *Angew. Chem. Int. Ed.* 53 (2014) 8056–8059.
- [17] S.H. Yang, K.B. Lee, B. Kong, J.H. Kim, H.S. Kim, I.S. Choi, *Angew. Chem. Int. Ed. Engl.* 48 (2009) 9160–9163.
- [18] S.H. Yang, E.H. Ko, Y.H. Jung, I.S. Choi, *Angew. Chem. Int. Ed.* 50 (2011) 6115–6118.
- [19] S.H. Yang, E.H. Ko, I.S. Choi, *Langmuir* 28 (2012) 2151–2155.
- [20] P.Q. Duan, T.T. Huang, W. Xiong, L. Shu, Y.L. Yang, C.Y. Shao, X.R. Xu, W.M. Ma, R.K. Tang, *Langmuir* 33 (2017) 2454–2459.
- [21] L.S.H. Chong, J.Y. Zhang, K.S. Bhat, D. Yong, J. Song, *Biomaterials* (2021) 266.
- [22] H. Furukawa, K.E. Cordova, M. O’Keeffe, O.M. Yaghi, *Science* 341 (2013) 974.
- [23] P. Horcajada, R. Gref, T. Baati, P.K. Allan, G. Maurin, P. Couvreur, G. Férey, R.E. Morris, C. Serre, *Chem. Rev.* 112 (2012) 1232–1268.
- [24] C. Doonan, R. Ricco, K. Liang, D. Bradshaw, P. Falcaro, *Acc. Chem. Res.* 50 (2017) 1423–1432.
- [25] R. Ricco, C. Pfeiffer, K. Sumida, C.J. Sumbly, P. Falcaro, S. Furukawa, N.R. Champness, C.J. Doonan, *CrystEngComm* 18 (2016) 6532–6542.
- [26] R.C. Huxford, K.E. deKrafft, W.S. Boyle, D.M. Liu, W.B. Lin, *Chem. Sci.* 3 (2012) 198–204.
- [27] J. Xu, H. Shimakoshi, Y. Hisaeda, J. Organomet. Chem. 782 (2015) 89–95.
- [28] F.K. Shieh, S.C. Wang, C.I. Yen, C.C. Wu, S. Dutta, L.Y. Chou, J.V. Morabito, P. Hu, M.H. Hsu, K.C. Wu, C.K. Tsung, *J. Am. Chem. Soc.* 137 (2015) 4276–4279.
- [29] K. Liang, R. Ricco, C.M. Doherty, M.J. Styles, S. Bell, N. Kirby, S. Mudie, D. Haylock, A.J. Hill, C.J. Doonan, P. Falcaro, *Nat. Commun.* 6 (2015).
- [30] W. Morris, W.E. Briley, E. Auyeung, M.D. Cabezas, C.A. Mirkin, *J. Am. Chem. Soc.* 136 (2014) 7261–7264.
- [31] K.M.L. Taylor, W.J. Rieter, W.B. Lin, *J. Am. Chem. Soc.* 130 (2008) 14358–+.
- [32] S.B. Li, M. Dharmawardana, R.P. Welch, Y.X. Ren, C.M. Thompson, R.A. Smaldone, J.J. Gassensmith, *Angew. Chem. Int. Ed.* 55 (2016) 10691–10696.
- [33] K. Liang, J.J. Richardson, J. Cui, F. Caruso, C.J. Doonan, P. Falcaro, *Adv. Mater.* 28 (2016) 7910–7914.
- [34] Z. Ji, H. Zhang, H. Liu, O.M. Yaghi, P. Yang, *Proc. Natl. Acad. Sci. U. S. A.* 115 (2018) 10582–10587.
- [35] A. Phan, C.J. Doonan, F.J. Uribe-Romo, C.B. Knobler, M. O’Keeffe, O.M. Yaghi, *Accounts Chem. Res.* 43 (2010) 58–67.
- [36] Y.C. Pan, Y.Y. Liu, G.F. Zeng, L. Zhao, Z.P. Lai, *Chem. Commun.* 47 (2011) 2071–2073.
- [37] F.J. Lyu, Y.F. Zhang, R.N. Zare, J. Ge, Z. Liu, *Nano Lett.* 14 (2014) 5761–5765.
- [38] C.Z. Wang, H.C. Sun, J.Y. Luan, Q.S. Jiang, S. Tadepalli, J.J. Morrissey, E.D. Kharasch, S. Singamaneni, *Chem. Mater.* 30 (2018) 1291–1300.
- [39] N.K. Maddigan, A. Tarzia, D.M. Huang, C.J. Sumbly, S.G. Bell, P. Falcaro, C.J. Doonan, *Chem. Sci.* 9 (2018) 4217–4223.
- [40] C. Zhang, J.F. Huang, J.C. Zhang, S.Y. Liu, M.K. Cui, B.L. An, X.Y. Wang, J.H. Pu, T.X. Zhao, C.H. Fan, T.K. Lu, C. Zhong, *Mater. Today* 28 (2019) 40–48.
- [41] X.Y. Wang, J.H. Pu, B.L. An, Y.F. Li, Y.Q. Shang, Z.J. Ning, Y. Liu, F. Ba, J.M. Zhang, C. Zhong, *Adv. Mater.* 30 (2018) 10.
- [42] J.F. Huang, S.Y. Liu, C. Zhang, X.Y. Wang, J.H. Pu, F. Ba, S. Xue, H.F. Ye, T.X. Zhao, K. Li, Y.Y. Wang, J.C. Zhang, L.H. Wang, C.H. Fan, T.K. Lu, C. Zhong, *Nat. Chem. Biol.* 15 (2019) 34.

- [43] H.L. Wang, S.F. He, X.D. Qin, C.E. Li, T. Li, *J. Am. Chem. Soc.* 140 (2018) 17203–17210.
- [44] Z.J. Wang, Y. Fu, Z.Z. Kang, X.G. Liu, N. Chen, Q. Wang, Y.Q. Tu, L.H. Wang, S.P. Song, D.S. Ling, H.Y. Song, X.Q. Kong, C.H. Fan, *J. Am. Chem. Soc.* 139 (2017) 15784–15791.
- [45] S. Brown, J.P.S. Maria, S. Walker, in: S. Gottesman (Ed.), *Annual Review of Microbiology*, vol. 67, 2013, pp. 313–336, vol. 67.
- [46] K.E. Eboigbodin, C.A. Biggs, *Biomacromolecules* 9 (2008) 686–695.
- [47] K.E. Eboigbodin, J.J. Ojeda, C.A. Biggs, *Langmuir* 23 (2007) 6691–6697.
- [48] W. Morris, C.J. Doonan, H. Furukawa, R. Banerjee, O.M. Yaghi, *J. Am. Chem. Soc.* 130 (2008) 12626+.
- [49] T.X. Yang, T.S. Chung, *J. Mater. Chem.* 1 (2013) 6081–6090.
- [50] M. Rohde, *Microbiol. Spectr.* 7 (2019).
- [51] K. Liang, R. Ricco, C.M. Doherty, M.J. Styles, S. Bell, N. Kirby, S. Mudie, D. Haylock, A.J. Hill, C.J. Doonan, P. Falcaro, *Nat. Commun.* 6 (2015) 8.
- [52] S. Gao, J.W. Hou, Z.Y. Deng, T.S. Wang, S. Beyer, A.G. Buzanich, J.J. Richardson, A. Rawal, R. Seidel, M.Y. Zulkifli, W.W. Li, T.D. Bennett, A.K. Cheetham, K. Liang, V. Chen, *Inside Chem.* 5 (2019) 1597–1608.
- [53] K. Liang, J.J. Richardson, C.J. Doonan, X. Mulet, Y. Ju, J. Cui, F. Caruso, P. Falcaro, *Angew. Chem. Int. Ed. Engl.* 56 (2017) 8510–8515.
- [54] J.H. Park, K. Kim, J. Lee, J.Y. Choi, D. Hong, S.H. Yang, F. Caruso, Y. Lee, I.S. Choi, *Angew. Chem. Int. Ed.* 53 (2014), 12420+.
- [55] H.K. Baca, C. Ashley, E. Carnes, D. Lopez, J. Flemming, D. Dunphy, S. Singh, Z. Chen, N.G. Liu, H.Y. Fan, G.P. Lopez, S.M. Brozik, M. Werner-Washburne, C.J. Brinker, *Science* 313 (2006) 337–341.
- [56] I. Canton, N.J. Warren, A. Chahal, K. Amps, A. Wood, R. Weightman, E. Wang, H. Moore, S.P. Armes, *ACS Cent. Sci.* 2 (2016) 65–74.
- [57] Z.X. Kang, L.L. Fan, D.F. Sun, *J. Mater. Chem.* 5 (2017) 10073–10091.
- [58] X.B. Liu, T. Yue, K. Qi, Y.B. Qiu, B.Y. Xia, X.P. Guo, *Chin. Chem. Lett.* 31 (2020) 2189–2201.
- [59] X. Wang, J. Pu, Y. Liu, F. Ba, M. Cui, K. Li, Y. Xie, Y. Nie, Q. Mi, T. Li, L. Liu, M. Zhu, C. Zhong, *Natl. Sci. Rev.* 6 (2019) 929–943.
- [60] L.M. Bjorklund, R. Sanchez-Pernaute, S.M. Chung, T. Andersson, I.Y.C. Chen, K.S. McNaught, A.L. Brownell, B.G. Jenkins, C. Wahlestedt, K.S. Kim, O. Isacson, *Proc. Natl. Acad. Sci. U. S. A.* 99 (2002) 2344–2349.